The Journal of Chemical Physics

Ce in the +4 oxidation state: Anion photoelectron spectroscopy and photodissociation of small $Ce_xO_yH_z^-$ molecules

Cite as: J. Chem. Phys. **147**, 104303 (2017); https://doi.org/10.1063/1.4996133
Submitted: 14 July 2017 . Accepted: 28 August 2017 . Published Online: 13 September 2017

Josey E. Topolski, Jared O. Kafader, and Caroline Chick Jarrold

Ce in the +4 oxidation state: Anion photoelectron spectroscopy and photodissociation of small $Ce_xO_yH_z^-$ molecules

Josey E. Topolski,[1] Jared O. Kafader,[2] and Caroline Chick Jarrold[1,a)]
[1]*Department of Chemistry, Indiana University, 800 East Kirkwood Avenue, Bloomington, Indiana 47405, USA*
[2]*Proteomic Center of Excellence, Northwestern University, 2170 Campus Dr., Evanston, Illinois 60208-2850, USA*

(Received 14 July 2017; accepted 28 August 2017; published online 13 September 2017)

The anion photoelectron (PE) spectra of a range of small mono-cerium molecular species, along with the $Ce_2O_4^-$ and $Ce_3O_6^-$ stoichiometric clusters, are presented and analyzed with the support of density functional theory calculations. A common attribute of all of the neutral species is that the Ce centers in both the molecules and clusters are in the +4 oxidation state. In bulk ceria (CeO_2), an unoccupied, narrow 4*f* band lies between the conventional valence (predominantly O 2*p*) and conduction (Ce 5*d*) bands. Within the CeO_2^-, $CeO_3H_2^-$, and $Ce(OH)_4^-$ series, the PE spectra and computational results suggest that the Ce 6*s*-based molecular orbital is the singly occupied HOMO in CeO_2^- but becomes destabilized as the Ce 4*f*-local orbital becomes stabilized with increasing coordination. CeO_3^-, a hyperoxide, undergoes photodissociation with 3.49 eV photon energy to form the stoichiometric neutral CeO_2 and O^-. In the CeO_2^-, $Ce_2O_4^-$,and $Ce_3O_6^-$ stoichiometric cluster series, the 6*s* destabilization with 4*f* stabilization is associated with increasing cluster size, suggesting that a bulk-like band structure may be realized with fairly small cluster sizes. The destabilization of the 6*s*-based molecular orbitals can be rationalized by their diffuse size relative to Ce—O bond lengths in a crystal structure, suggesting that 6*s* bands in the bulk may be relegated to the surface. *Published by AIP Publishing.* [http://dx.doi.org/10.1063/1.4996133]

I. INTRODUCTION

Ceria's unique ability to easily uptake and conduct oxygen, via the interconversion of its +4 and +3 oxidation states, allows for its use in a variety of applications, one of which being a platinum catalytic support for the water-gas shift reaction ($H_2O + CO \rightarrow H_2 + CO_2$).[1–3] Several studies of ceria-supported first row transition[4] or precious metals[5,6] have demonstrated an increase in catalytic activity of the metals relative to non-ceria supported metals, with further enhancement of activity observed with ceria nanoparticle support. From a molecular standpoint, the electronic structures of molecules with a lanthanoid atom are both complex and interesting because of the partially occupied 4*f* subshell, which is non-bonding but close in energy to the 5*d* and 6*s* atomic orbitals. Thus, many studies have aimed to understand the unique electronic structure of cerium oxides employing methods such as ligand field theory,[7] fluorescence spectroscopies,[8–11] infrared vibrational predissociation spectroscopy,[12] matrix infrared spectroscopy,[13,14] x-ray absorption spectroscopy,[15] and photodissociation.[16]

In an effort to understand the electronic structure of cerium oxide clusters and their chemical properties, we recently completed studies on the reactivity of cerium suboxide clusters toward water[17] and used density functional theory calculations alongside anion photoelectron (PE) spectroscopy to investigate the electronic structures of Ce,[18] CeO and $Ce(OH)_2$,[19] Ce_xO_y (x = 2–5, y = 0–4),[20] and $Ce_xO_yH_z$ (x = 2–3, y = 3–7, z = 1–5) cluster anions and neutrals.[21] In addition to this work, Aubriet *et al.* have studied cerium oxyhydroxide cluster formation with mass spectrometry and density functional theory modeling.[22] Beyond water, the reactivity of cerium oxides with carbon and nitrogen oxides,[23–28] sulfur dioxide,[29] molecular oxygen,[30] and hydrocarbons[31,32] has also been investigated.

The anion PE spectra of Ce-containing molecules and clusters in which the Ce centers are in lower-than bulk oxidation states are distinguished by large photodetachment cross sections associated with the transition to the ground neutral state, low neutral electron affinities, all in the range of 0.7–1.2 eV, and photoelectron angular distributions consistent with detachment from orbitals with predominant 6*s* character, resulting in *p*-wave photoelectrons (i.e., parallel transitions).[33] Based on the work of O'Malley and Beck,[34] the photodetachment cross section of transitions involving Ce^- atomic anion 6*s* orbitals is much greater than detachment transitions associated with 4*f* orbitals. Therefore, anion photodetachment of Ce-containing molecular anions in which the Ce centers in the neutral species are in the +4 oxidation state is expected to be challenging because the HOMO of the anion, based on the relative energies of the 4*f*, 5*d*, and 6*s* bands in bulk Ce_2O_3 and CeO_2,[35,36] could be Ce local-4*f* atomic orbitals. Additionally, the low photodetachment cross section would be coupled with substantial structural changes upon photodetachment, due to the +1 change in effective nuclear charge (Z_{eff}) on the Ce-center.

a)Author to whom correspondence should be addressed: cjarrold@indiana.edu

In the present report, we consider the anion PE spectra of several small molecules and clusters in which the Ce centers in the neutrals are in the +4 oxidation state. Specifically, we present and analyze the PE spectra of CeO_2^-, CeO_3^-, $CeO_3H_2^-$, $Ce(OH)_4^-$, $Ce_2O_4^-$, and $Ce_3O_6^-$. In the initial anion states, except for CeO_3^-, one Ce center is in the +3 oxidation state. A qualitative description of the electronic and molecular structures is supported by DFT (density functional theory) calculations, though we note that, in certain cases, lack of agreement between the spectra and spectroscopic parameters gleaned from the computation results underscores the need for caution when treating complex species with common and accessible computational methods. Our results show how the relative energies of the Ce 4*f* and 6*s* orbitals are affected by the molecular bonding environment.

II. METHODS

A. Experimental methods

Clusters are produced, mass analyzed, and undergo photoelectron detachment in an experimental apparatus described previously.[37,38] The molecules described below were produced in several variations of a laser-ablation/pulsed molecular beam source based on the design of Dietz *et al.*[39] The surface of a rotating target disk was ablated with 3-5 mJ/pulse of the second harmonic output of a Nd:YAG laser (532 nm, or 2.33 eV) with a repetition rate of 30 Hz. The target used for production of CeO_2^-, CeO_3^-, $Ce_2O_4^-$, and $Ce_3O_6^-$ was a pressed ceria (CeO_2) powder (Sigma Aldrich), and a pressed Ce metal (Sigma Aldrich, 99.9%) was used in the production of the other molecular species described below. In both cases, the powder was pressed into a disk mold with up to 3 metric tons using a hydraulic press. Upon ablation, the resulting plasma was entrained in a pulse of ultra-high purity helium (UHP He) issued from a pulsed molecular beam valve. Except for the production of CeO_2^-, the gas mixture was swept through a 3-mm diameter, 25 mm-long clustering channel. Specifically, for the production of $CeO_3H_2^-$ and $Ce(OH)_4^-$, a second pulsed beam valve injected H_2O seeded in UHP He as the ions passed through the clustering channel. For the production of CeO_2^-, the clustering channel was altogether removed from the ion source.

The resulting gas mixtures expanded into the vacuum chamber and passed through a 3-mm skimmer, and the anions were accelerated into a 1.2-m time-of-flight mass spectrometer. After passing through a 3-mm mass defining slit, the ions passed through a laser interaction region before colliding with a dual microchannel plate (MCP) detector assembly. The anions were selectively photodetached using one of the harmonics (532 nm or 2.33 eV; 355 nm or 3.49 eV; 266 nm or 4.66 eV) of a second Nd:YAG laser timed to intersect a specific ion of interest. A small fraction of the photoelectrons traveled the length of a 1-m long field-free drift tube and were detected with a second MCP detector. The drift times were recorded with a digitizing oscilloscope and converted to electron kinetic energy, e^-KE, calibrated with the well-known PE spectra of O^- and OH^-.

The e^-KE values, which reflect the relative energies of the neutral states relative to the initial anion state via

$$e^-KE = h\nu - EA - E_{internal}^{neutral} + E_{internal}^{anion}, \quad (1)$$

where EA is the neutral electron affinity, were converted to electron binding energy (e^-BE) values, which are photon-independent, with the relationship

$$e^-BE = h\nu - e^-KE. \quad (2)$$

All of the PE spectra shown below plot electron counts as a function of e^-BE.

Spectra were collected using two detachment laser polarizations, $\theta = 0°$ (parallel) and $\theta = 90°$ (perpendicular), to the direction of the photoelectron drift tube. The ratio of the resulting intensities was used to calculate the asymmetry parameter, $\beta(E)$, which provides experimental point of comparison to previously collected PE spectra of cerium suboxide clusters, giving insight into the molecular orbital origin of the detached electron. The asymmetry parameter is approximated from the following expression:

$$\beta = \frac{(I_0 - I_{90})}{(0.5I_0 + I_{90})}. \quad (3)$$

The PE spectra presented below were collected with 1 480 000 laser shots for CeO_2^- (2.33 eV), 1 160 000 laser shots for CeO_2^- (3.49 eV), 2 600 000 laser shots for $CeO_3H_2^-$ (2.33 eV), 2 320 000 (3.49 eV), 1 680 000 laser shots for $Ce(OH)_4^-$, 640 000 laser shots for CeO_3^-, 120 000 laser shots for $Ce_2O_4^-$, and 280 000 laser shots for $Ce_3O_6^-$.

B. Computational details

Molecular and electronic structures of anion and neutral clusters were explored using the GAUSSIAN 09 suite of electronic structure programs.[40] The unrestricted B3LYP hybrid density functional method was employed with the Stuttgart relativistic, small core atomic natural orbital/effective core potential (ANO/ECP) basis set which has a 28-electron pseudopotential and an atomic natural orbital contracted Gaussian basis for the valence electrons, (14*s*,13*p*,10*d*,8*f*,6*g*)/[6*s*,6*p*,5*d*,4*f*,3*g*], for cerium[41] and the aug-cc-pVTZ Dunning correlation consistent basis set for hydrogen and oxygen.[42] Numerous structural isomers in a range of possible spin states (evens for one charge state and odds for the other charge state) were explored. Possible structural isomers were determined using chemical intuition and results from studies that were discussed previously.

For direct comparison with the anion PE spectra, for each low-lying anion, the adiabatic detachment energy (ADE) was computed as the difference between the zero-point corrected total energy of the optimized anion and a one-electron accessible optimized neutral state, and the vertical detachment energy (VDE), which corresponds to the energy within an electronic transition at which the Franck-Condon overlap between the initial anion and final neutral states is maximum, was computed by the difference between a single-point energy calculation on the neutral constrained to the structure of the anion and the total energy of the optimized anion.

III. RESULTS

Figure 1 shows mass spectra of ions generated in the several variations of source conditions. Figure 1(a) shows the distribution of clusters generated from ablation of a pressed ceria (CeO_2) target. CeO_3^-, $Ce_2O_4^-$, and $Ce_3O_6^-$, along with larger clusters not shown, dominate the mass spectrum when a clustering channel is attached to the ablation source; CeO_2^- could only be produced when the channel was removed. Figure 1(b) shows the initial ion distribution for species with a single Ce-atom generated from ablation of the Ce-metal target (black trace), along with the species generated after introduction of H_2O into the clustering channel (blue trace). As noted previously, the PE spectra of atomic Ce^- (Ref. 18) and the suboxide CeO^- and $CeO_2H_2^-$ molecules[19] were reported previously. The molecules and clusters targeted for this study are labeled in bold face. We were unable to photodetach $CeO_5H_6^-$.

A. PE spectra and computational results on CeO_2^-, $CeO_3H_2^-$, $Ce(OH)_4^-$, and CeO_3^-

Figure 2 shows the PE spectra of the monometallic molecular anions for which Ce in the neutral molecule is in the +4 oxidation state. In the case of CeO_3^-, Ce is also in the +4 oxidation state. For the remaining three molecular anions, Ce is in the +3 oxidation state. Of these four molecular anions, CeO_2^- had the characteristically high photodetachment cross section. The remaining spectra shown in Fig. 2 are sums of the spectra obtained with both laser polarizations, to improve signal to noise.

The intense band in the CeO_2^- spectra, labeled X, is at slightly lower e^-BE than CeO^- and the other larger suboxide systems but is a parallel transition, similar to the suboxides.

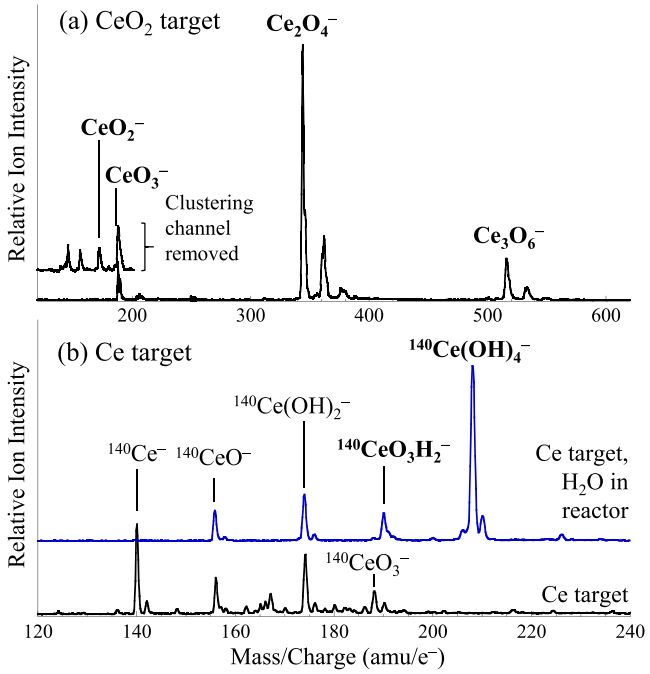

FIG. 1. Mass spectrum of $CeO_yH_z^-$ clusters generated via ablation of a (a) pressed ceria target and (b) pressed cerium target without (black) and with (blue) water introduced into the clustering channel. Masses shown in bold text are addressed in this manuscript.

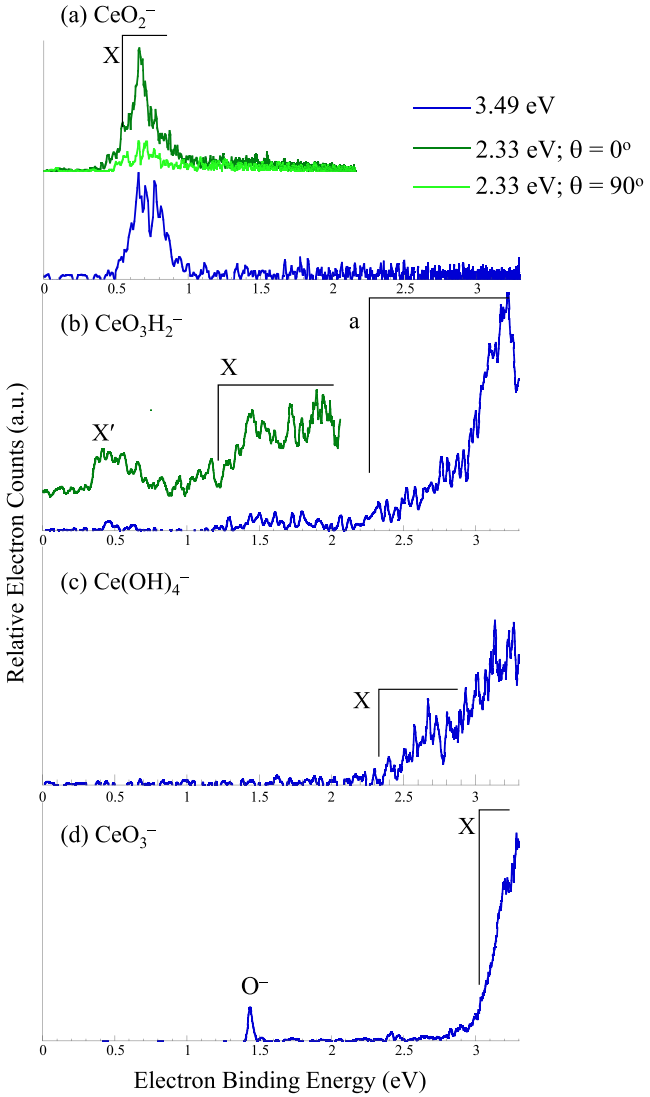

FIG. 2. PE spectra of $CeO_yH_z^-$ molecular anions. See Table I for a summary of e^-BE values and asymmetry parameters.

The PE spectra of $CeO_3H_2^-$, shown in Fig. 2(b), exhibit two broad, low-intensity bands, labeled X′ and X with origins at 0.36(1) eV and 1.19(2) eV, respectively, along with what is presumably an excited state transition, labeled a, at 2.24 eV e^-BE. There is continuum signal between bands X and a, making the origin of band a difficult to identify. The PE spectrum of $Ce(OH)_4^-$, which was presented as a counter-example to cerium suboxo-hydroxide anion PE spectra reported previously,[21] exhibits no electron signal at e^-BE values below the approximately 2.4 eV onset of a noisy, rising edge (labeled X). The CeO_3^- PE spectrum shown in Fig. 2(d) also exhibits a higher e^-BE onset of signal at 2.97(2) eV, in addition to a sharp peak at 1.46 eV, attributable to O^-,[43] indicating that two-photon process, CeO_3^- photodissociation to O^- + CeO_2, followed by photodetachment of the O^- photofragment, is occurring. Table I summarizes e^-BE's of all of the transitions in these spectra, along with asymmetry parameters.

As expected, DFT calculations predict doublet ground electronic states for the anions and singlet states for the neutrals. The molecular structures for the anions are depicted in

TABLE I. Summary of experimentally observed transitions for $Ce_xO_yH_z^-$ clusters. For each band, the anisotropy parameter, adiabatic detachment energy, vertical detachment energy, and tentative assignment are listed.

Band	Asymmetry parameter	ADE/VDE	Tentative assignments
CeO_2^-			
X	1.1	0.66(10)/0.66(2)	$^1A_1 \leftarrow {}^2A_1$
$CeO_3H_2^-$			
A	0.1	2.24(3)/...	$^3A' \leftarrow {}^2A'$
X	0.3	1.19(2)/1.44(1)	$^1A' \leftarrow {}^2A'$
X′	0.4	0.36(1)/0.44(1)	$^2A' \leftarrow {}^3A''$
$Ce(OH)_4^-$			
X	0.0	2.38(1)/...	$^1A_1 \leftarrow {}^2A$
CeO_3^-			
X	0.6	2.97(2)/...	$^1A_1 \leftarrow {}^2A_1$
O^-	−0.4	1.46	$O \leftarrow O^-$
$Ce_2O_4^-$			
X	1.2	0.85(5)/1.00(1)	$^1A_1 \leftarrow {}^2A_1$

Fig. 3, along with depictions and relative energies of the singly occupied HOMO, the LUMO, and the highest doubly occupied orbital. Additional details, including several structural parameters and electronic terms for both the anions and neutrals, are summarized in Table II. The supplementary material includes all electronic states of all structures that converged in the calculations, with their relative energies.

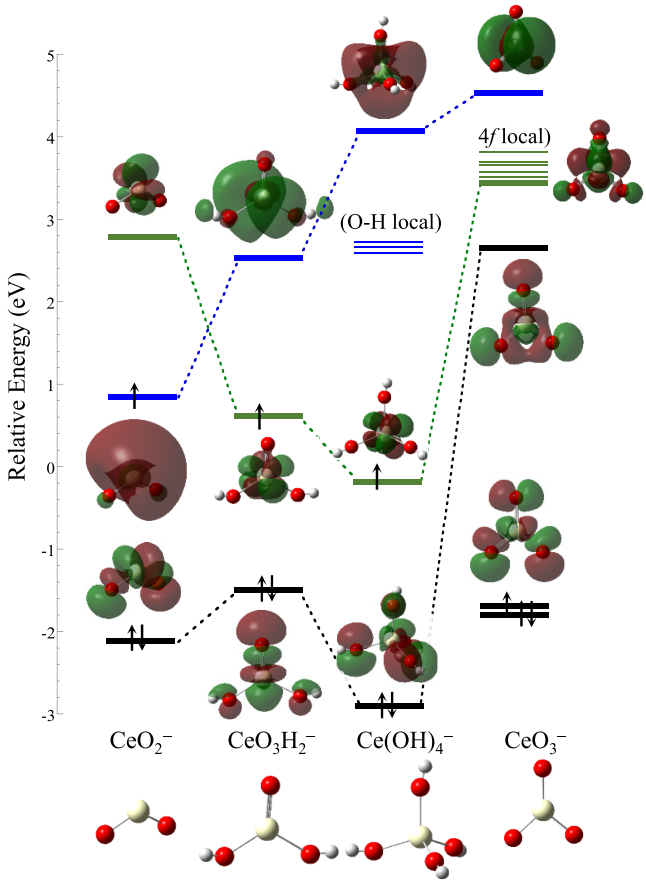

FIG. 3. Calculated orbital energies and occupancies of the lowest energy structures and electronic states of CeO_2^-, $CeO_3H_2^-$, $Ce(OH)_4^-$, and CeO_3^-, summarized in Table II. The supplementary material includes the comprehensive computational results.

Immediately evident from Fig. 3 is that the singly occupied HOMO predicted for CeO_2^- is Ce 6*s*-like, with the LUMO being Ce 4*f*-like. For $CeO_3H_2^-$ and $Ce(OH)_4^-$, the Ce-center is formally in the +3 oxidation state, but the singly occupied HOMO for both is a Ce 4*f* orbital, while the MO with the most Ce 6*s* (or 6*s*-5*d* hybrid) character is higher in energy. The singly occupied HOMO of the hyperoxide CeO_3^- molecule is, as expected, predominantly O 2*p* orbitals. The three O centers are sharing the 4 electrons from Ce, plus the extra electron in the anion, resulting in a single hole in the molecular orbitals largely described as combinations of the O 2*p* orbitals. The calculated transition energies for these species are summarized in Table II.

1. CeO_2^-/CeO_2

The lowest energy state found computationally for CeO_2^-, the $^2A_1$ state (orbital occupancy depicted in Fig. 3), is calculated to be 0.54 eV lower in energy than the lowest energy neutral in the $^1A_1$ state, which is accessed by detaching the electron from the 6*s*-like orbital. This value is in good agreement with the observed transition energy, 0.66(10) eV. Excited anion states in which one of the 4*f* orbitals is occupied rather than the 6*s*-like orbital (Table II) lie above the calculated detachment continuum, but are informative in that their structures feature much longer Ce—O bond lengths than the ground anion and neutral states due to the lower Z_{eff} on Ce. Figure 4(a) shows a simulation based on the spectroscopic parameters (black trace) superimposed on the experimental spectrum obtained with 2.33 eV. The calculations appear to underestimate the change in Ce—O bond length; the progression in the 790 cm^{-1} symmetric stretch mode in the simulation is less extended than the observed progression (ω_1'' = 764 cm^{-1}, ΔQ = 0.09 Å $amu^{1/2}$; a more complete listing of all spectroscopic parameters is included in the supplementary material). The unresolved progression in the 86 cm^{-1} bend mode, however, reproduces the experimental peak width reasonably well. We note here that CeO_2^- could only be produced under very hot source conditions. The overall profile of the experimental spectrum could be simulated by assuming ΔQ = 0.2 Å $amu^{1/2}$, T ~ 2500 K.

2. $CeO_3H_2^-/CeO_3H_2$ and $Ce(OH)_4^-/Ce(OH)_4$

Because the singly occupied HOMO's in $CeO_3H_2^-$ and $Ce(OH)_4^-$ are Ce 4*f* orbitals, the photodetachment cross sections are expected to be very small. The calculated ADE of the ground state $^2A' \rightarrow {}^1A'$ transition in the $CeO_3H_2^-$ spectrum is 1.17 eV, while the ADE associated with detaching an electron from the 2*p*-like HOMO-1 orbital, the $^2A' \rightarrow {}^3A'$, is predicted to be 2.88 eV. The VDE's calculated for both transitions are ca. 0.7 eV higher in energy, reflecting large Ce—O and Ce—OH bond length changes. While simulating broad, featureless transitions is generally uninformative, we generated two simulations using the Ce=O and symmetric Ce—OH stretch frequencies of the anion and two neutral

TABLE II. Summary of density functional theory calculation results for $Ce_xO_yH_z$ anion and neutral clusters. The point group, electronic term symbol, relative energy, and $\langle S^2 \rangle$ values are listed for each state. Several structural parameters are included. Complete structural parameters and totally symmetric vibrational frequencies are included in the supplementary material. The lowest energy one-e^- transitions are included with their corresponding adiabatic and vertical detachment energies. The experimental adiabatic and vertical detachment energies have been included for reference.

State	Relative energy (eV)	$\langle S^2 \rangle$	Structure parameters r_{Ce-O} (Å)/$\angle_{O-Ce-O}$(deg)	Relevant one-e$^-$ transitions	ADE/VDE (eV)	Experimental ADE/VDE (eV)
CeO_2						
C_{2v} $^1A_1$	0.54	0.00	1.820/140	$^1A_1 \leftarrow {}^2A_1$	0.54/0.61	0.66(10)/0.66(2)
CeO_2^-						
C_{2v} $^2A_2$ ($4f_\Delta$)	0.72	0.75	1.961/116			
C_{2v} $^2B_1$ ($4f_\Phi$)	0.66	0.75	1.967/119			
C_{2v} $^2A_1$ (6*s*)	0.00	0.75	1.856/122			
CeO_2H						
C_s $^4A''$	3.49	3.75	2.162/110			
C_s $^2A'$	0.54	0.75	1.848/118	$^2A' \leftarrow {}^3A''$	0.54/2.46	
CeO_2H^-						
C_s $^1A'$	0.78	0.00	1.835/108			
C_s $^3A''$	0.00	2.00	1.885/113			
CeO_3						
C_{2v} $^1A_1$	3.35	0.00	1.824/87	$^1A_1 \leftarrow {}^2A_1$	3.35/3.93	2.97(2)/...
CeO_3^-						
C_{2v} $^2A_1$	0.00	0.77	1.945/102			
CeO_3H_2						
C_s $^3A'$	2.88	2.01	2.085/113	$^3A' \leftarrow {}^2A'$	2.88/3.54	2.24(3)/...
C_s $^1A'$	1.17	0.00	1.803/111	$^1A' \leftarrow {}^2A'$	1.17/1.92	1.19(2)/1.44(1)
$CeO_3H_2^-$						
C_s $^2A''$ ($4f_\Pi$)	0.02	0.75	1.921/122			
C_s $^2A'$ ($4f_\Delta$)	0.00	0.75	1.918/122			
$Ce(OH)_4$						
T_d $^1A_1$	2.20	0.00	2.093/109	$^1A_1 \leftarrow {}^2A$	>2.20/...	2.38(1)/...
$Ce(OH)_4^-$						
C_1 ^2A (t.s.)	0.00	0.75	2.237/109			
Ce_2O_4						
C_{3v} $^1A_1$	1.57	0.00	1.808/69	$^1A_1 \leftarrow {}^2A_1$	1.52/2.15	
C_{2v} $^1A_1$ (*cis*)	1.20	0.00	1.809/75	$^1A_1 \leftarrow {}^2A''$	1.07/1.98	
				$^1A_1 \leftarrow {}^2A_1$	0.96/1.07	0.85(5)/1.00(1)
C_s $^1A'$ (*trans*)	1.12	0.00	1.812/75	$^1A' \leftarrow {}^2A'$	1.12/1.85	
$Ce_2O_4^-$						
C_{2v} $^2A_1$ (*cis*) (t.s.)	0.24	0.76	1.866/77			
C_s $^2A''$ (*cis*)	0.13	0.75	1.918/72			
C_{3v} $^2A_1$	0.05	0.75	1.879/75			
C_s $^2A'$ (*trans*)	0.00	0.75	1.878/82			
Ce_3O_6						
C_1 ^1A (*chain*)	2.88	0.00	1.809/75	$^1A \leftarrow {}^2A$	2.08/2.96	
C_1 ^1A	2.61	0.00	1.806/95	$^1A \leftarrow {}^2A$	1.81/2.72	...
C_s $^1A'$	2.27	0.00	1.813/112	$^1A' \leftarrow {}^2A'$	2.27/3.22	...
$Ce_3O_6^-$						
C_1 ^2A	0.80	0.75	1.861/144			
C_1 ^2A (*chain*)	0.80	0.75	1.863/81			
C_s $^2A'$	0.00	0.75	1.868/108			

states (other modes such as Ce—O—H bends and twists, and umbrella motion, are active, resulting in overall congestion and loss of resolved vibrational structure), applying physically meaningful normal coordinate displacements *vis à vis* the calculated bond length changes, until the simulated VDE-ADE difference matched the calculated VDE-ADE difference. (The spectroscopic parameters used to generate the simulations are included in the supplementary material.) The results of the simulation are shown as a black trace in Fig. 4(b) superimposed on the PE spectrum obtained with 3.49 eV (dotted blue trace).

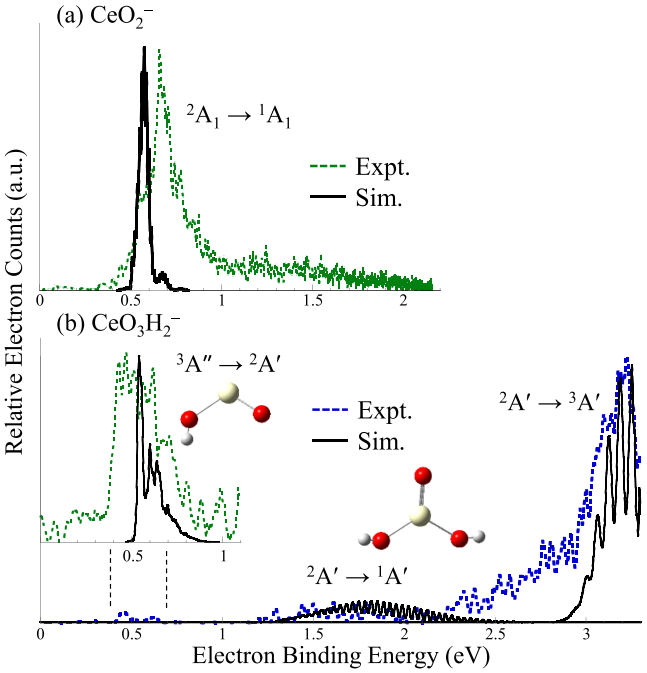

FIG. 4. Spectra simulated from calculated results (black) overlaid on experimental spectra (blue or green) are shown for (a) CeO_2^- and (b) $CeO_3H_2^-$. The simulation parameters used are included in the supplementary material.

The origins of the two bands were set to the calculated values, and the intensities of the bands were scaled to approximate the appearance of the spectrum.

While the simulations do not definitively support the assignment and the calculations, they are qualitatively consistent with the observed spectrum, with the exception of band X′ at 0.36 eV e^-BE. Band X′ cannot be explained by the calculated transition energies from the lowest energy anion structure found. One potential explanation is photodissociation followed by photodetachment, as is observed in the CeO_3^- PE spectrum. Band X′ does not resemble the PE spectra of Ce^-,[18] CeO^-, $CeOH_2^-$,[19] CeO_2^-,or CeO_3^- (*vide supra*), or OH^-,[44] leaving CeO_2H^- as a potential photofragment. Calculations on CeO_2H^-, summarized in the supplementary material, predict that the Ce center has a 4*f* 6*s* orbital occupancy, with an accompanying low binding energy characteristic of detachment of the electron from the 6*s*-like orbital. The simulation (black trace) shown in the inset of Fig. 4(b) superimposed on the spectrum obtained with 2.33 eV photon energy (green dotted trace) is based on the calculated $^3A'' \rightarrow {}^2A'$ lowest energy transition and is much narrower than the observed transition. However, we note that photofragments are often generated with high internal energy, which would result in spectral congestion due to electronic and vibrational hot bands.

An unsatisfying aspect of this explanation is the lack of OH^- detachment signal. If $CeO_3H_2^-$ dissociates to CeO_2H^- + OH, given the much higher EA of OH, the lack of discernable OH^- signal is surprising. We therefore also consider the possibility that an excited state of $CeO_3H_2^-$, such as a state associated with single occupancy of the 5*d*-6*s*-like orbital, is long-lived and present in the ion beam. The larger photodetachment cross section and smaller structural change associated with detachment of an electron from a diffuse non-bonding orbital would compensate for the low abundance of this state. In either explanation, the photoelectron angular distribution of band X′ is consistent with detachment of an electron from a 6*s*-like orbital.

The high binding energy and abundance of $Ce(OH)_4^-$ (Fig. 1) suggest that the molecule is stable. Results of DFT calculations predict that the tetra-hydroxide structure shown in Fig. 3 is more stable than the only other chemically intuitive $CeO_2^-\cdot(H_2O)_2$ structure by 1.36 eV. One caveat is that a minimum energy $Ce(OH)_4^-$ structure did not converge in calculations; the structure shown has a single imaginary frequency of −18.68 cm^{-1}. However, this structure was found to be 2.2 eV below the corresponding neutral; the binding energy would therefore be greater than, but close to, 2.2 eV. The experimental binding energy of 2.38 eV is consistent with this value, and the tetrahedral structure is likely correct. Again, as summarized in Table II, the Ce—OH bond lengths change significantly upon photodetachment. As noted previously,[21] the Ce—OH bonds are highly ionic, and the +1 change in Z_{eff} resulting from detachment of an electron from the local 4*f* results in Ce—OH bond contraction. The anisotropy parameter is consistent with electron detachment from a 4*f*-like molecular orbital.

3. CeO_3^-/CeO_3

The results of DFT calculations on both the anion and neutral states of CeO_3, summarized in Fig. 3 and Table II, predict C_{2v} structures, consistent with previous reports by Wu *et al.*[27] The $^2A_1 \rightarrow {}^1A_1$ transition was calculated to be 3.35 eV, at the cut-off energy of our electron detection. The rising edge of signal in the PE spectrum is possibly due to vibrational and electronic hot bands. The singly occupied HOMO and doubly occupied HOMO-1 are nearly degenerate, which would give rise to close-lying doublet anion states, with transitions to close-lying singlet and triplet neutral states. The Ce 4*f* subshell is unoccupied in both the anion and neutral, and the 4*f* orbital energies are therefore nearly degenerate, lying between the O 2*p*-based LUMO and the higher lying Ce 5*d*/6*s*-based molecular orbital, as depicted schematically in Fig. 3.

B. PE spectra and computational results on $Ce_2O_4^-$ and $Ce_3O_6^-$

Figure 5 shows the PE spectra of [Fig. 5(a)] $Ce_2O_4^-$ obtained using 3.49 eV photon energies, with both parallel and perpendicular polarizations (dark and light blue, respectively), and Fig. 5(b) shows the result of collecting electrons from detachment of $Ce_3O_6^-$ using 4.66 eV photon energy for 280 000 laser shots. The spectrum obtained using 3.49 eV photon energy was similarly flat. In contrast, the PE spectrum of $Ce_2O_4^-$ exhibits one electronic transition, labeled X, at 0.85(5) eV with an asymmetry parameter of 1.2, both of which are consistent with the characteristic Ce 6*s*-based molecular orbital detachment observed for the suboxide species and CeO_2^-.

Figure 6 shows the molecular structures, orbital energies, and occupancies calculated for the three stoichiometric clusters. (CeO_2^- is reproduced in this figure for direct comparison.)

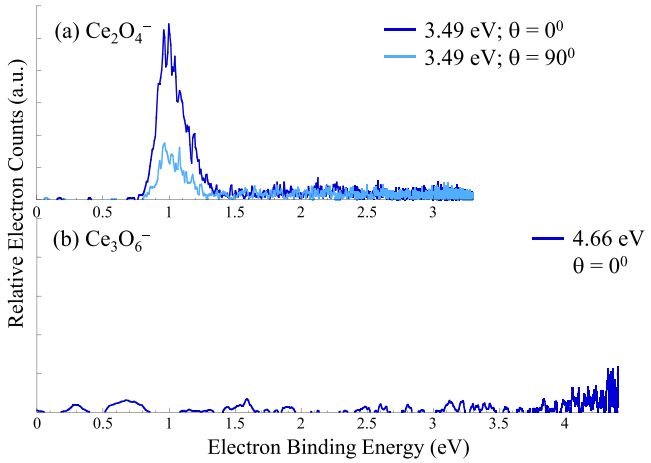

FIG. 5. [(a) and (b)] PE spectra of $Ce_xO_{2x}^-$ stoichiometric clusters. Table I summarizes e^-BE values and asymmetry parameters.

Included are three close-lying structures that converged for $Ce_2O_4^-$: two with two bridging O-atoms, and a terminal O-atom on each Ce center in *cis*- or *trans*-configuration. The *cis*-structure was calculated to be 0.13 eV higher in energy than the *trans*-structure, which is the global minimum. An additional low-lying C_{3v} structure with three bridging O-atoms and a single terminal O atom, resembling a tadpole, converged 0.05 eV higher in energy than the *trans*-structure. Table II includes relative energies, transition energies, and several bond lengths. Higher lying structures for this and all other molecules in this study are included in the supplementary material.

The structures calculated for $Ce_2O_4^-$ are similar to those calculated for $Ce_2O_4^+$, for which two versions of a *trans*-like structure and a tadpole structure were all found to be within 0.1 eV.[31] All three of $Ce_2O_4^-$ structures have a unique

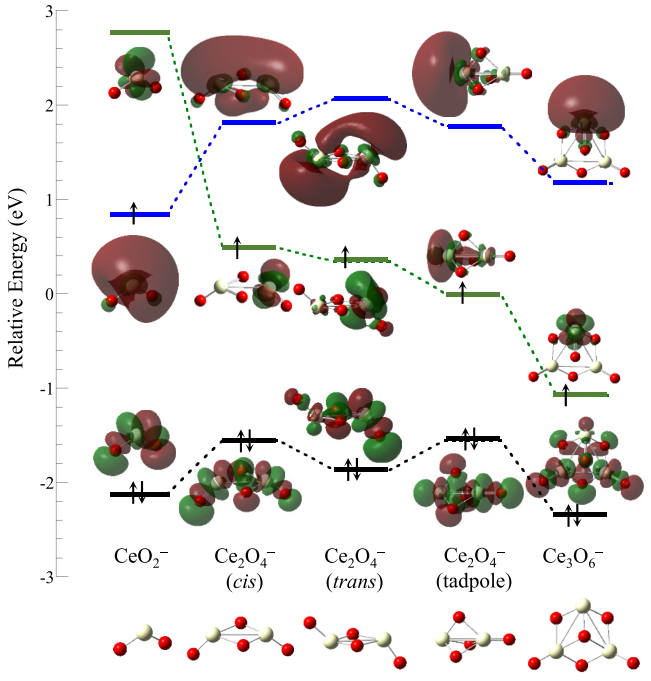

FIG. 6. Calculated orbital energies and occupancies of CeO_2^-, the close-lying $Ce_2O_4^-$ (*cis*), $Ce_2O_4^-$ (*trans*), and $Ce_2O_4^-$ (tadpole) structures, and the lowest energy structure found for $Ce_3O_6^-$.

Ce^{3+} center with a singly occupied 4*f* orbital. While the two Ce centers in the tadpole structure are necessarily in different oxidation states, it is surprising that the HOMOs of both the *trans* and *cis* structures, according to the computational results, are broken-symmetry. Moreover, none of the computational results agree with the experimental spectrum. The calculated ADE values and VDE-ADE differences are higher than the observed transition. (The ADE for the tadpole structure is 1.52 eV, which is outside the 0.3 eV window of error generally accepted for these calculations.) To underscore how the VDE-ADE energy difference is inconsistent with the observed spectrum, a simulation based on the *trans* structure is shown in Fig. 7 (gray trace), superimposed on the experimental spectrum obtained using 2.33 eV photon energy (green dotted trace). Based on the ADE/VDE values for the *cis* structure (Table II), the predicted spectrum of the *cis* structure would be slightly higher in energy and more vibrationally extended. Further, since the HOMOs of all three competitive anions are Ce 4*f*-local orbitals, the photodetachment cross section is expected to be much lower than what was experienced experimentally.

Because asymmetric Ce oxidation states in what ostensibly would appear to be a symmetric molecule (e.g., the *trans* and *cis* structures of $Ce_2O_4^-$) are chemically unintuitive, we also performed calculations on the *cis* $Ce_2O_4^-$ structure, constrained to C_{2v} symmetry. This structure did converge 0.11 eV higher than the optimized structure, with one imaginary frequency associated with the b_2 symmetry bridging oxygen motion that correlates to the asymmetric *cis* structure. The HOMO predicted for this structure is the in-phase combination of the symmetric Ce 6*s* orbitals, shown in Fig. 7. A simulation based on this structure is included as the solid black trace; the agreement is clearly better. We address this result in Sec. IV.

The lowest energy structure found computationally for $Ce_3O_6^-$ is similar to the structure determined for $Ce_3O_4^-$,[12,20] with the addition of two terminal O-atoms, leaving one unique Ce center, the locus of the singly occupied Ce 4*f* orbital. The ground state structure calculated for $Ce_3O_6^+$ by Wu *et al.*[31] is similar, but with *trans* terminal oxygens rather than the *cis*

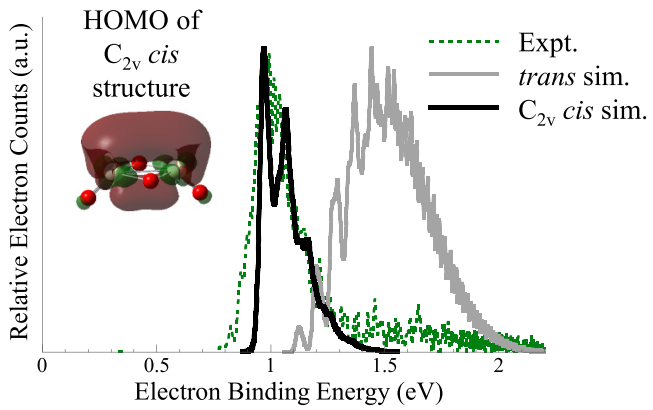

FIG. 7. Spectrum simulated from calculated spectroscopic parameters for the lowest energy *trans* structure of $Ce_2O_4^-$ (gray) and a *cis* structure confined to C_{2v} symmetry (black) overlaid on experimental spectrum obtained with 2.33 eV photon energy (green). The simulation parameters used are included in the supplementary material.

structure determined here for the anion. Nagata *et al.* calculated the ground state structure to have two central O-atoms (one above and the other below the Ce_3 triangle), one bridging O-atom between adjacent Ce centers, and one terminal oxygen.[24]

The lowest-energy $^2A' \rightarrow {}^1A'$ transition ADE is calculated to be 2.27 eV and is therefore energetically accessible with 3.49 eV photon energy. However, as is expected for detachment of an electron from a 4*f*-local orbital, the small photodetachment cross sections coupled with significant structural rearrangement results in the disappointing spectrum shown in Fig. 5(b).

IV. DISCUSSION

The anion PE spectra coupled with DFT calculations of this series of molecules and clusters in which the Ce centers in the neutral are all in the +4 oxidation state underscore how the ligand environment of the Ce center affects the relative energies of the 4*f* and 6*s* orbitals in the anion and showcase the striking differences in cross sections of diffuse and local molecular orbitals. In Fig. 3, the progression of 6*s*-based molecular orbital destabilization and Ce 4*f* orbital stabilization accompanies an increase in coordination. The bent CeO_2^- structure accommodates the 6*s*-like HOMO, which is also likely stabilized by the large dipole moment of CeO_2. Indeed, the HOMO of CeO_2^- resembles a localized dipole bound electron orbital.[45] Substitution of two hydroxyl groups for one Ce=O double bond maintains the Ce oxidation state but interrupts the large space, and the 6*s*-like HOMO, hybridized with a 5*d* orbital, has bifurcation of the amplitude by the near-planar molecular structure. Further, because the Ce—OH bonds are more ionic than Ce=O bonds,[21] the Ce partial charge is greater in CeO_3H_2 [computed atomic polar tensor (APT) charge is +2.73] than in CeO_2 (computed APT charge is 2.26), which stabilizes the 4*f* orbital occupancy.

The $Ce_xO_{2x}^-$ ($x = 1$–3) stoichiometric cluster series offers a glimpse into the evolution of band structure in ceria from small molecular CeO_2 toward the bulk. Figure 6 suggests the first steps in this evolution. As noted before, bulk CeO_2 band structure features a narrow, unoccupied 4*f* band situated between the valence and conduction bands, the latter generally described as a Ce 5*d* band. With bulk Ce_2O_3, each Ce center has a singly occupied 4*f* orbital; the narrow 4*f* band is at the Fermi level.[35,36] While, on the basis of the PE spectrum and the computational results, the HOMO of triatomic CeO_2^- (LUMO of CeO_2) is unambiguously a diffuse 6*s*-like orbital, the experimental spectrum of $Ce_2O_4^-$ is at odds with the computational results, which minimally suggests that the 6*s*-like and 4*f* local orbitals are close in energy. With the incremental increase in cluster size to $Ce_3O_6^-$, the calculations predict that the 4*f*-local orbital on the unique Ce center is stabilized relative to the 6*s* orbital, which is localized on the same unique Ce center. Considering the bulk band structure, as the lattice is more extended, the 5*d* band at some point becomes lower in energy than the 6*s* band, which is destabilized because the diffuse 6*s* orbitals are spatially more extended than the Ce—O bonds in the bulk, and could only exist on the surface.

The computational results on $Ce_2O_4^-/Ce_2O_4$ are unique in that they failed to correctly predict that the HOMO of the anion is a 6*s*-based MO, which is inferred from the PE spectrum (the rule of thumb being the following: 6*s* detachment is super, and 4*f* is frustrating). Figures 3 and 6 both show a progression of 4*f* orbital occupancy stabilization and 6*s* orbital occupancy destabilization with increasing coordination (Fig. 3) or size (Fig. 6). It is possible that in $Ce_2O_4^-/Ce_2O_4$, the two possible occupancies are so close that small errors in the calculation tip the computational results to the incorrect occupancy. Alternatively, it is possible that both states are in fact energetically competitive and populated in the ion beam (either one being the ground state), and only the state with 6*s* orbital occupancy is observed experimentally. Indeed, if band X′ in the PE spectrum of $CeO_3H_2^-$ is an electronic hot band originating from an anion state with a singly occupied 5*d*-6*s* hybrid orbital, both $Ce_2O_4^-$ and $CeO_3H_2^-$ lie at the crossing point between the 6*s* and 4*f* energies. Higher level calculations may resolve this question.

The competitiveness of states with 4*f* versus 6*s* orbital occupancy has implications for other interesting properties of these and similar molecules. For example, because the contracted 4*f* orbital angular momentum may not be quenched in these species, the magnetic moment should be sensitive to whether the 4*f*-like or 6*s*-like molecular orbital is occupied, given $\mu = (2\mathbf{S} + \mathbf{L})\,\mu_B$, where μ_B is the Bohr magneton, **S** and **L** are the spin and total angular momenta, respectively.[46,47] Further, inasmuch as these molecules might lend insight into the catalytic properties of ceria, 4*f* versus 6*s* occupancy of a Ce center in the +3 oxidation state will govern the distance at which overlap between the Ce-local orbitals and a target molecule occurs.

Finally, we comment on photofragmentation as it relates to the question of band X′ in the PE spectrum of $CeO_3H_2^-$. Unambiguous evidence of photodissociation was observed in the PE spectrum of CeO_3^-, yielding O^- and CeO_2. Photodissociation of clusters in other studies has frequently resulted in stoichiometries that reflect units of the bulk material.[16,48–53] Since the only photofragment to which band X′ could potentially be assigned, based on elimination of all other photofragments, is the non-stoichiomentric CeO_2H^- molecule, whose e^-BE is more than 1 eV lower than the corresponding OH neutral, we lean towards assigning band X′ in the PE spectrum of $CeO_3H_2^-$ to an electronic hot band, placing the excited state at approximately 0.8 eV higher in energy than the ground state, assuming that the neutral ground state is accessed in both bands X and X′.

V. CONCLUSIONS

The anion PE spectra of a range of small mono-cerium oxo-hydroxy molecular species, along with the $Ce_2O_4^-$ and $Ce_3O_6^-$ stoichiometric clusters, are presented and analyzed with the support of density functional theory calculations. The motivation for this study arose from our previous observations that all cerium suboxide clusters exhibit fundamentally similar photodetachment transitions that are characteristic of detachment from Ce 6*s*-based molecular orbitals. That is, the detachment cross section is large, the transitions are parallel,

and the binding energy is low, *ca*. 1 eV or less. All small, cerium suboxide cluster anions apparently have 6*s*-based HOMO's.

A common attribute of all of the neutral species in the current study is that the Ce centers in both the molecules and clusters are in the favored bulk oxide +4 oxidation state. In bulk ceria (CeO_2), an unoccupied, narrow 4*f* band lies between the conventional valence (predominantly O 2*p*) and conduction (Ce 5*d*) bands, with the Ce 6*s* band apparently lying higher in energy. Within the CeO_2^-, $CeO_3H_2^-$, and $Ce(OH)_4^-$ series, CeO_2^- is unique in that it exhibits the characteristic Ce 6*s*-based MO electron detachment transition. This result and the PE spectra of more coordinated molecules combined with computational results suggest that while the Ce 6*s*-based molecular orbital is the singly occupied HOMO in CeO_2^-, this orbital becomes destabilized, and the Ce 4*f*-local orbital becomes stabilized with increasing coordination. This trend appears to be due to a combination of steric destabilization of the diffuse Ce 6*s*-based orbital and increased positive charge on the Ce center when mixed ionic-covalent Ce═O bonds are substituted by more ionic Ce—OH bonds. CeO_3^-, a hyperoxide, unambiguously undergoes both photodissociation with 3.49 eV photon energy to form the stoichiometric neutral CeO_2 and O^- and direct photodetachment.

In the CeO_2^-, $Ce_2O_4^-$, and $Ce_3O_6^-$ stoichiometric cluster series, the 6*s* destabilization with 4*f* stabilization is associated with increasing cluster size, suggesting that a bulk-like band structure may be realized with fairly small cluster sizes. The destabilization of the 6*s*-based molecular orbitals can be rationalized by their diffuse size relative to Ce—O bond lengths in a crystal structure, suggesting that 6*s* bands in the bulk may be relegated to the surface.

SUPPLEMENTARY MATERIAL

See supplementary material for a listing of computational output-based spectroscopic parameters used in the spectral simulations, summaries of all structures and spin states for each molecular species described herein, and input structures.

ACKNOWLEDGMENTS

This work was supported by the National Science Foundation Grant No. CHE-1265991.

[1] R. J. Gorte, AIChE J. **56**, 1126 (2010).
[2] L. Saraf, C. M. Wang, V. Shutthanandan, Y. Zhang, O. Marina, D. R. Baer, S. Thevuthasan, P. Nachimuthu, and D. W. Lindle, J. Mater. Res. **20**, 1295 (2011).
[3] T. Montini, M. Melchionna, M. Monai, and P. Fornasiero, Chem. Rev. **116**, 5987 (2016).
[4] Y. Li, Q. Fu, and M. Flytzani-Stephanopoulos, Appl. Catal., B **27**, 179 (2000).
[5] T. Bunluesin, R. J. Gorte, and G. W. Graham, Appl. Catal., B **15**, 107 (1998).
[6] A. Luengnaruemitchai, S. Osuwan, and E. Gulari, Catal. Commun. **4**, 215 (2003).
[7] R. W. Field, Ber. Bunsen. Phys. Chem. **86**, 771 (1982).
[8] C. Linton, M. Dulick, and R. W. Field, J. Mol. Spectrosc. **78**, 428 (1979).
[9] C. Linton, M. Dulick, R. W. Field, P. Carette, and R. F. Barrow, J. Chem. Phys. **74**, 189 (1981).
[10] L. A. Kaledin, J. E. Mccord, and M. C. Heaven, J. Mol. Spectrosc. **40**, 158 (1993).
[11] C. Linton, M. Dulick, R. W. Field, P. Carette, P. C. Leyland, and B. F. Barrow, J. Mol. Spectrosc. **102**, 441 (1983).
[12] A. M. Burow, T. Wende, M. Sierka, R. Wlodarczyk, J. Sauer, P. Claes, L. Jiang, G. Meijer, P. Lievens, and K. R. Asmis, Phys. Chem. Chem. Phys. **13**, 19393 (2011).
[13] S. D. Gabelnick, G. T. Reedy, and M. G. Chasanov, J. Chem. Phys. **60**, 1167 (1974).
[14] S. P. Willson and L. Andrews, J. Phys. Chem. A **103**, 3171 (1999).
[15] H. Tetsuichiro, E. Kazuhiro, A. Masashi, I. Tomonori, S. Shun, A. Kota, and T. Akira, J. Phys. B: At., Mol. Opt. Phys. **49**, 075101 (2016).
[16] S. T. Akin, S. G. Ard, B. E. Dye, H. F. Schaefer, and M. A. Duncan, J. Phys. Chem. A **120**, 2313 (2016).
[17] J. A. Felton, M. Ray, S. E. Waller, J. O. Kafader, and C. C. Jarrold, J. Phys. Chem. A **118**, 9960 (2014).
[18] J. A. Felton, M. Ray, and C. C. Jarrold, Phys. Rev. A **89**, 033407 (2014).
[19] M. Ray, J. A. Felton, J. O. Kafader, J. E. Topolski, and C. C. Jarrold, J. Chem. Phys. **142**, 064305 (2015).
[20] J. O. Kafader, J. E. Topolski, and C. C. Jarrold, J. Chem. Phys. **145**, 154306 (2016).
[21] J. E. Topolski, J. O. Kafader, M. Ray, and C. C. Jarrold, J. Mol. Spectrosc. **336**, 1 (2017).
[22] F. Aubriet, J. J. Gaumet, W. A. de Jong, G. S. Groenewold, A. K. Gianotto, M. E. McIlwain, M. J. Van Stipdonk, and C. M. Leavitt, J. Phys. Chem. A **113**, 6239 (2009).
[23] T. Nagata, K. Miyajima, and F. Mafuné, J. Phys. Chem. A **119**, 10255 (2015).
[24] T. Nagata, K. Miyajima, R. A. Hardy, G. F. Metha, and F. Mafuné, J. Phys. Chem. A **119**, 5545 (2015).
[25] T. Nagata, K. Miyajima, and F. Mafuné, J. Phys. Chem. A **119**, 1813 (2015).
[26] S. Hirabayashi and M. Ichihashi, J. Phys. Chem. A **117**, 9005 (2013).
[27] X.-N. Wu, X.-L. Ding, S.-M. Bai, B. Xu, S.-G. He, and Q. Shi, J. Phys. Chem. C **115**, 13329 (2011).
[28] M. Zhou, X. Jin, and J. Li, J. Phys. Chem. A **110**, 10206–10211 (2006).
[29] Z.-X. Zhou, L. N. Wang, Z.-Y. Li, S.-G. He, and T.-M. Ma, J. Phys. Chem. A **120**, 3843 (2016).
[30] S. Hirabayashi and M. Ichihashi, Chem. Phys. Lett. **564**, 16 (2013).
[31] X.-N. Wu, Y.-X. Zhao, W. Xue, Z.-C. Wang, S.-G. He, and X.-L. Ding, Phys. Chem. Chem. Phys. **12**, 3984 (2010).
[32] C. Heinemann, H. H. Cornehl, D. Schröder, M. Dolg, and H. Schwarz, Inorg. Chem. **35**, 2463 (1996).
[33] A. Sanov, Annu. Rev. Phys. Chem. **65**, 341 (2014).
[34] S. M. O'Malley and D. R. Beck, Phys. Rev. A **74**, 042509 (2006).
[35] J. L. F. Da Silva, M. V. Ganduglia-Pirovano, J. Sauer, V. Bayer, and G. Kresse, Phys. Rev. B **75**, 045121 (2007).
[36] P. J. Hay, R. L. Martin, J. Uddin, and G. E. Scuseria, J. Chem. Phys. **125**, 034712 (2006).
[37] V. D. Moravec and C. C. Jarrold, J. Chem. Phys. **108**, 1804 (1998).
[38] S. E. Waller, J. E. Mann, and C. C. Jarrold, J. Phys. Chem. A **117**, 1765 (2013).
[39] T. G. Dietz, M. A. Duncan, D. E. Powers, and R. E. Smalley, J. Chem. Phys. **74**, 6511 (1981).
[40] M. J. Frisch, G. W. Trucks, H. B. Schlegel, G. E. Scuseria, M. A. Robb, J. R. Cheeseman, G. Scalmani, V. Barone, B. Mennucci, G. A. Petersson, H. Nakatsuji, M. Caricato, X. Li, H. P. Hratchian, A. F. Izmaylov, J. Bloino, G. Zheng, J. L. Sonnenberg, M. Hada, M. Ehara, K. Toyota, R. Fukuda, J. Hasegawa, M. Ishida, T. Nakajima, Y. Honda, O. Kitao, H. Nakai, T. Vreven, J. A. Montgomery, Jr., J. E. Peralta, F. Ogliaro, M. J. Bearpark, J. Heyd, E. N. Brothers, K. N. Kudin, V. N. Staroverov, R. Kobayashi, J. Normand, K. Raghavachari, A. P. Rendell, J. C. Burant, S. S. Iyengar, J. Tomasi, M. Cossi, N. Rega, N. J. Millam, M. Klene, J. E. Knox, J. B. Cross, V. Bakken, C. Adamo, J. Jaramillo, R. Gomperts, R. E. Stratmann, O. Yazyev, A. J. Austin, R. Cammi, C. Pomelli, J. W. Ochterski, R. L. Martin, K. Morokuma, V. G. Zakrzewski, G. A. Voth, P. Salvador, J. J. Dannenberg, S. Dapprich, A. D. Daniels, Ö. Farkas, J. B. Foresman, J. V. Ortiz, J. Cioslowski, and D. J. Fox, GAUSSIAN 09, Revision D.01, Gaussian, Inc., Wallingford, CT, USA, 2009.
[41] X. Cao and M. Dolg, J. Chem. Phys. **115**, 7348 (2001).
[42] T. H. Dunning, J. Chem. Phys. **90**, 1007 (1989).
[43] S. J. Cavanagh, S. T. Gibson, M. N. Gale, C. J. Dedman, E. H. Roberts, and R. B. Lewis, Phys. Rev. A **76**, 052708 (2007).
[44] J. B. Kim, P. G. Wenthold, and W. C. Lineberger, J. Chem. Phys. **108**, 830 (1998).

[45]M. Gutowski, K. D. Jordan, and P. Skurski, J. Phys. Chem. A **102**, 2624 (1998).
[46]G. L. Gutsev, C. W. Weatherford, K. G. Belay, B. R. Ramachandran, and P. Jena, J. Chem. Phys. **138**, 164303 (2013).
[47]X. Xing, A. Hermann, X. Kuang, M. Ju, C. Lu, Y. Jin, X. Xia, and G. Maroulis, Sci. Rep. **6**, 19656 (2016).
[48]K. S. Molek, T. D. Jaeger, and M. A. Duncan, J. Chem. Phys. **123**, 144313 (2005).
[49]S. E. Kooi and A. W. Castleman, J. Phys. Chem. A **103**, 5671 (1999).
[50]R. C. Bell, K. A. Zemski, K. P. Kerns, H. T. Deng, and A. W. Castleman, J. Phys. Chem. A **102**, 1733 (1988).
[51]K. S. Molek, Z. D. Reed, A. M. Ricks, and M. A. Duncan, J. Phys. Chem. A **111**, 8080 (2007).
[52]K. S. Molek, C. Anfuso-Cleary, and M. A. Duncan, J. Phys. Chem. A **112**, 9238 (2008).
[53]Z. D. Reed and M. A. Duncan, J. Phys. Chem. A **112**, 5354 (2008).